# Atom interferometry with polarizing beam splitters

H. Hinderthür, A. Pautz, F. Ruschewitz, K. Sengstock, and W. Ertmer

*Institut für Quantenoptik der Universität Hannover, Welfengarten 1, D-30167 Hannover, Germany*

A special kind of atomic beam splitter using a four-level atomic system in combination with polarized light fields is demonstrated. These specific atom optical elements are used to operate an atom interferometer where the beam-splitting mechanism acts selectively on specific paths only and therefore allows for several different interferometer geometries. Based on a Ramsey-Bordé configuration, the experimental data show considerably better accuracy and a contrast enhanced by 65% compared to the two-level interferometer. Our concept appears to be especially interesting in the context of metrological aspects in matter-wave interferometry. [S1050-2947(98)04506-5]

## I. INTRODUCTION

The recent development in atom interferometry has opened up different areas in fundamental and applied research [1]. Typical de Broglie wavelengths for atoms are much smaller than those of electrons, neutrons, or light waves. Moreover, the internal structure of atoms offers additional degrees of freedom. Atom interferometry, therefore, has gained great interest in the construction of highly stable frequency standards, accelerometers, or gravitational detectors, studies of atomic properties, and the investigation of fundamental quantum mechanical questions, to name only a few prominent applications [1,2]. In the context of Bose-Einstein condensation, atom interferometry is expected to become an important tool to test quantum statistical effects.

In recent years several versions of atom interferometers have been realized [3–11]. In particularly the so-called Ramsey-Bordé interferometer has been the basis for a series of precision measurements [1,6,7,12–16]. For this class of interferometers the beam-splitting process is due to the discrete exchange of photon momenta between two levels of an atom and a resonant light field producing an entanglement of the atomic internal and external states within the interferometer. This allows the selective access to one arm of the interferometer without the need for spatial separation between the two arms, though this spatial separation also exists.

Within a purely two-level atomic system as it is originally assumed for the Ramsey-Bordé interferometer [17], the interaction between the beam splitters and the atomic de Broglie wave splits each incoming wave into two paths. The beam-splitting process is not selective to a certain interferometer arm. As a consequence, a large number of partial waves appear at the interferometer exit. Waves that do not take part in the successive interference process lead to a high background signal. Two closed loops represent independent interferometers corresponding to the two recoil components. The interference signals from these two recoil components overlap, which may result in undesired line-pulling effects if the fringe period does not correspond to the recoil splitting.

In this paper we present an interferometer scheme that is based on path-selective atomic beam splitters (PSABs). Our concept is based on a Ramsey-Bordé atom interferometer where the internal manifold of atomic levels is extended from the originally used two-level system to a four-level system. This opens the possibility to realize more complex beam-splitting geometries and by this means more efficient interferometer configurations, e.g., an increase in the amplitude of the interfering de Broglie waves and a reduction of the background signal. Thus the observed interference signals of a thermal atomic beam show increased contrast and a better accuracy compared to the conventional Ramsey-Bordé interferometer based on a two-level system. Optical Ramsey-Bordé interferometry with three internal states has recently been demonstrated in a conceptionally different way to realize a three-beam atom interferometer [19] and to observe crossover resonances [20].

In the following section of the paper we discuss the general principle of the path-selective beam-splitting process and the concept of a pure Mach-Zehnder atom interferometer. In Sec. III we give a more detailed calculation of the interferometer signals followed by a discussion of results of a numerical simulation for typical experimental parameters. Section IV presents recent experimental results of this kind of atom interferometer with magnesium atoms. We conclude in Sec. V.

## II. GENERAL CONCEPT

It has been shown by Bordé that the transfer of Ramsey's classical method of separated microwave fields to an experimental configuration in which a two-level atom interacts with two pairs of counterpropagating parallel and equidistant resonant laser waves constitutes a matter-wave interferometer [17]. This is illustrated in Fig. 1(a). The $y$ axis in the diagrams in Fig. 1 is magnified to show clearly the influence of the photon recoil. Therefore, we refer to these diagrams as ''photon recoil diagrams'' as proposed in [17]. The optical pulse area of the four subsequent laser interactions is expected to be $\Omega_{Rabi}\tau = \pi/2$, which corresponds to an atomic de Broglie wave beam splitter ratio of 50% for each interaction. The lifetime of the excited state has to be long compared to the time of flight of the atom through the interferometer so that spontaneous decay is negligible.
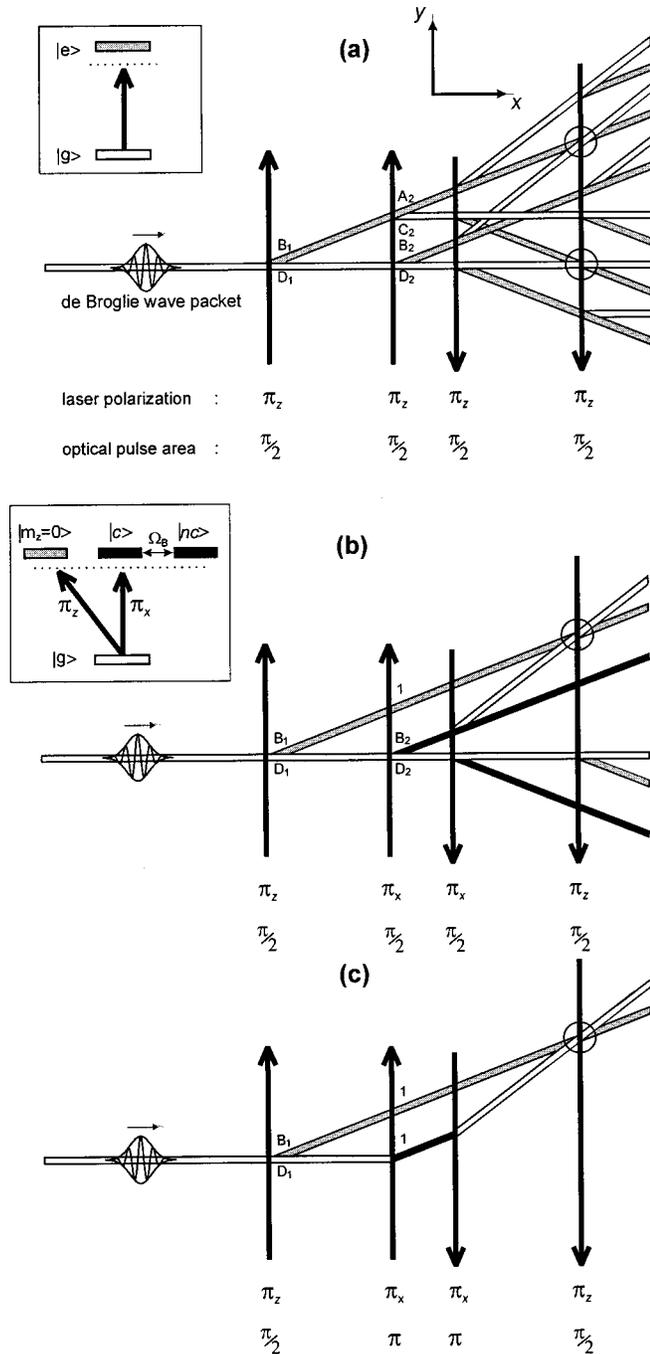
FIG. 1. Photon recoil diagrams of the different atom interferometer configurations. Atomic de Broglie wave packets coming from the left are split or deflected due to the exchange of single-photon momenta with the four laser fields. The transition coefficients for the first two interaction zones are indicated. Positions where closed loops join are labeled by circles. (a) Conventional two-level Ramsey-Bordé interferometer. (b) PSAB interferometer. (c) Mach-Zehnder interferometer.

For the two-level system the beam splitters do not act path selectively, i.e., for each interaction zone each incoming wave is split into two partial waves of equal amplitudes. At the interferometer exit this leads to 16 partial waves. Two closed loops form independent interferometers, the so-called high- and low-frequency recoil components. In Fig. 1 positions where the closed loops join are labeled by circles. The

probability of finding the atom in the excited state behind the fourth interaction zone typically shows two fringe systems according to the two recoil components with an oscillatory dependence on the laser frequency. These fringe systems are separated by twice the atomic photon recoil energy divided by the Planck constant $h$. Partial beams that leave the interferometer at different positions do not interfere because of the limited transverse atomic coherence. So an additional broad background is due to the open paths in Fig. 1 [18]. The dependence of the interference signal on the laser frequency is correctly explained in terms of energy and momentum conservation during the beam-splitting process [7].

In Fig. 1(b) a photon recoil diagram for an interferometer with path-selective beam splitters is indicated. The idea is based on the extension of the laser interaction to a four-level system of a $J = 0$ to $J' = 1$ transition with a long-lived $J' = 1$ state. Atoms in the $J' = 1$ ($m_J = \pm 1$) state couple to an electric-field vector that is parallel to the $x$ axis ($\pi_x$ polarized), whereas atoms in the $J' = 1$ ($m_J = 0$) state couple to field vectors that are parallel to the $z$ axis ($\pi_z$ polarized). Thus, in an atom interferometer an appropriate sequence of laser beam splitters with different linear polarizations allows for state-selective beam splitting of certain paths that are labeled by their internal quantum state $m_J$.

The polarization sequence of the four laser beams forming the interferometer setup indicated in Fig. 1(b) is $\pi_z$-$\pi_x$-$\pi_x$-$\pi_z$. After the interaction with the first beam splitter the excited partial wave is optically pumped to the $J' = 1$ ($m_J = 0$) state. This state does not interact with the following two beam splitters, which act only on the $J = 0$ and $J' = 1$ ($m_J = \pm 1$) state partial waves, respectively. As a consequence, the number of atomic waves in the interferometer is reduced by a factor of 2. In particular, the high-frequency recoil component is no longer closed. According to the reduced number of beam-splitting processes, the amplitudes of the remaining waves are increased, resulting in a higher interference signal of the low-frequency component.

In more detail the atomic beam-splitting ratio for each laser beam is governed by the optical pulse area. While for a pulse area of $\pi/2$, as assumed above, the atomic wave is split into two amplitudes of the same size, a laser interaction with a pulse area of $\pi$ generates a complete population transfer. The effect of this population inversion between the ground and the excited state on the atomic center-of-mass motion represents an entire deflection of the atom. In Fig. 1(c) the photon recoil diagram of an interferometer is indicated where the beam splitters are path selective and the inner two laser beams work as atomic deflectors. This can be realized by a polarization sequence $\pi_z$-$\pi_x$-$\pi_x$-$\pi_z$ and an optical pulse sequence $\pi/2$-$\pi$-$\pi$-$\pi/2$, respectively. Indeed, this scheme represents a pure Mach-Zehnder interferometer without any additional paths as well known from photon optics. Theoretically, the maximum achievable contrast for this device is 100%. This can be achieved, e.g., using laser-cooled monochromatic atoms, whereas for a thermal atomic beam setup the maximum contrast is reduced due to the atomic velocity distribution. This will be discussed in the following section.

## III. CALCULATION OF THE INTERFERENCE AMPLITUDES

In this section we will briefly outline the calculation of the interference amplitudes for the interferometer configurations

described above. According to the entanglement between the internal and external degrees of freedom for this kind of interferometry the interference signal is encoded in the internal state of the atom. Therefore, we have to consider the evolution of the internal atomic state due to the laser interaction.

In a two-level system the state vector consists of two components. Thus, for a single interaction region the transition from an incident state $|i\rangle = (\langle i|e\rangle, \langle i|g\rangle)$ to a final state $|f\rangle = (\langle f|e\rangle, \langle f|g\rangle)$ can be described by the matrix equation

$$|f\rangle = \begin{bmatrix} A & B \\ C & D \end{bmatrix} |i\rangle. \tag{1}$$

The coefficients $A$, $B$, $C$, and $D$ describe the transition probabilities following from the solution of the Schrödinger equation. They depend on the laser detuning, the two-level Rabi frequency, the atomic velocity, and the interaction time with the laser beams. For a detailed calculation see Ref. [18].

Considering all paths in Fig. 1(a), the final probability to find the atom at the interferometer exit in the excited state follows from subsequent multiplication of the transition coefficients along the different paths:

$$|\langle e|e\rangle|^2 = |B_4 C_3 A_2 B_1|^2 + |A_4 A_3 B_2 D_1|^2 + |B_4 D_3 C_2 B_1|^2$$

$$+ |A_4 B_3 D_2 D_1|^2 + |A_4 A_3 A_2 B_1 + e^{i\Phi_+} B_4 C_3 B_2 D_1|^2$$

$$+ |A_4 B_3 C_2 B_1 + e^{i\Phi_-} B_4 D_3 D_2 D_1|^2. \tag{2}$$

Here the indices denote the corresponding interaction region as exemplarily indicated in Fig. 1 for the first two laser zones. $\Phi_+$ and $\Phi_-$ are the overall resulting phase factors for the high- and low-frequency recoil components accumulated on the different paths in the interferometer. Each term in bars in Eq. (2) represents a certain path in the photon recoil diagram of Fig. 1(a). Exit ports in Fig. 1 that are spatially separated do not interfere and contribute to the background signal only. The first four terms of Eq. (2) describe this incoherent part of the signal due to all open paths, whereas the last two terms represent the interferences of the two recoil components resulting in a sinusoidal doublet structure. For idealized 50% beam splitters the magnitude of the transition amplitudes ($A,B,C,D$) is $1/\sqrt{2}$. Hence, from Eq. (2) it is easy to calculate an interference contrast, defined as the amplitude of the interference signal divided by the incoherent signal, of 25% for a single recoil component.

To describe the signal of the PSAB interferometer one has to calculate the state evolution within the $J=0$ to $J'=1$ transition for a sequence of four laser pulses with different linear polarizations. For reasons of simplicity we introduce the state basis

$$B = \{|g\rangle, |e_0\rangle, |e_c\rangle, |e_{nc}\rangle\} \quad \text{with} \quad |e_0\rangle = |m_z' = 0\rangle,$$

$$|e_c\rangle = 1/\sqrt{2}(|m_z' = +1\rangle - |m_z' = -1\rangle),$$

$$|e_{nc}\rangle = 1/\sqrt{2}(|m_z' = +1\rangle + |m_z' = -1\rangle), \tag{3}$$

where the states $|e_c\rangle$ and $|e_{nc}\rangle$ are linear combinations of the Zeeman states in the magnetic-field basis. In the basis of Eq.

(3) only three states take part in the laser interaction [see also inset in Fig. 1(b)]. Between the bright state $|e_c\rangle$ and the dark state $|e_{nc}\rangle$ there is a weak-coupling mechanism $\Omega_b$ due to small magnetic fields. We will discuss this in Sec. IV. To a good approximation the dark state remains unpopulated during the laser interaction and each single interaction of the atom with $\pi_z$- and $\pi_x$-polarized laser beams, respectively, can be described in terms of three-component state vectors [for example, $|i\rangle = (\langle i|e_0\rangle, \langle i|e_c\rangle, \langle i|g\rangle)$]:

$$|f\rangle = \begin{bmatrix} A & 0 & B \\ 0 & 1 & 0 \\ C & 0 & D \end{bmatrix}_{\pi_z} |i\rangle \tag{4a}$$

and

$$|f\rangle = \begin{bmatrix} 1 & 0 & 0 \\ 0 & A & B \\ 0 & C & D \end{bmatrix}_{\pi_x} |i\rangle. \tag{4b}$$

Note that each individual beam-splitting process can be effectively described as a two-level interaction according to
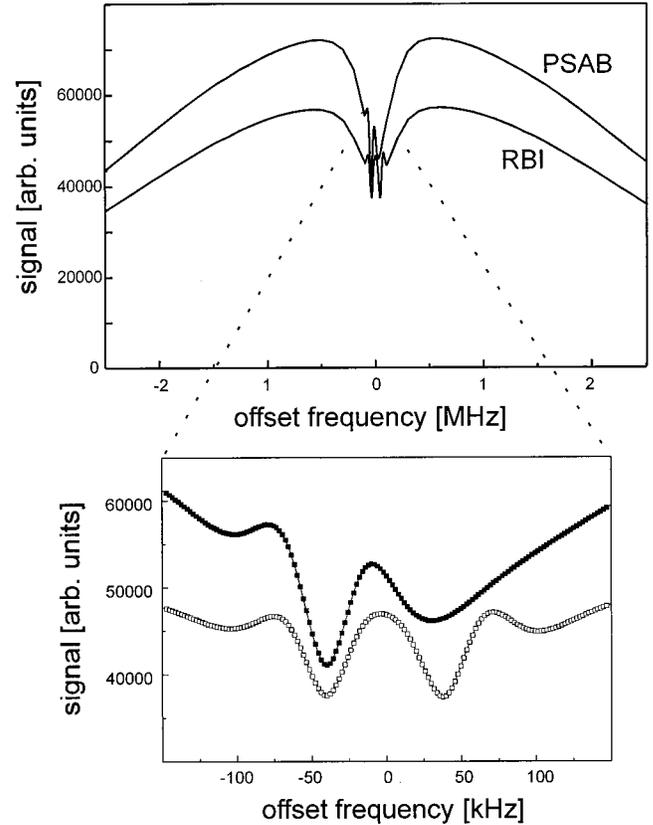


FIG. 2. Comparison of the signals calculated from Eqs. (2) and (5) for the two-level Ramsey-Bordé interferometer (RBI) (open squares) and the PSAB interferometer (solid squares). A Maxwell-Boltzmann velocity distribution is taken into account. The upper diagram shows the signal structure including the Doppler and Lamp-dip structure. The curves are calculated for identical experimental parameters (see the text).

the specific choice of basis. Subsequent application of Eqs. (4) then leads to the signal that corresponds to the PSAB interferometer

$$|\langle e|e\rangle|^2 = |A_3 B_2 D_1|^2 + |B_3 D_2 D_1|^2 + |B_4 D_3 D_2 D_1|^2$$
$$+ |A_4 B_1 + e^{i\Phi +} B_4 C_3 B_2 D_1|^2. \qquad (5)$$

Equation (5) resembles the reduced number of paths in the photon recoil diagram [Fig. 1(b)]. In contrast to Eq. (2), the high-frequency recoil component has disappeared and only one interference term remains. Both the incoherent amplitudes [first three terms on the right-hand side of Eq. (5)] and the amplitude of the interference term are increased compared to the two-level case. For idealized 50% beam splitters Eq. (5) leads to an interference contrast of 40% for the PSAB interferometer.

For the pure Mach-Zehnder interferometer [Fig. 1(c)] Eq. (5) is also valid. In this case the optical pulse area corresponds to $\Omega_{\text{Rabi}} \tau = \pi$ for the second and third interactions. For idealized beam splitters this leads to transition coefficients $B_2 = B_3 = C_2 = C_3 = 1$ and $A_2 = A_3 = D_2 = D_3 = 0$, respectively, which represents a complete population inversion.

The interferometer is dispersive in the sense that atoms with different longitudinal velocities contribute with different interference periodicities to the overall signal. This results in a "washing out" of the higher-order interference fringes [18]. A detailed explanation of this effect in terms of coherence length properties is given in [20]. The longitudinal velocities also determine the optical pulse area via the interaction time with the laser beams. Therefore, the signal contrast varies with the longitudinal velocity. Transverse velocity components, on the other hand, produce Doppler shifts resulting in a modification of the effective Rabi frequency. Thus both longitudinal and transverse velocity components of the thermal atomic beam generate a chromatic aberration and complicate the control of the atomic beam-splitter ratio. For this reason the extension of the PSAB interferometer to the pure Mach-Zehnder geometry as indicated in Fig. 1(c) is extremely difficult for a thermal beam ensemble. For interferometry in the time domain with laser-cooled atoms as described in [21] a contrast modulation of nearly 100% becomes possible.

In Fig. 2 interferometer signals for typical experimental conditions as described in detail in Sec. IV are plotted. The curves are modeled through Eqs. (2) and (5), where the longitudinal velocity distribution is a Maxwell-Boltzmann one. The coherent part of the signals is embedded into a broad saturation spectroscopic structure according to the fraction of de Broglie wave amplitudes that do not take part in the interference process. The open squares represent the typical doublet structure as known from two-level Ramsey-Bordé interferometry [see also Fig. 1(a)]. The constructive overlap of the two fringe systems leads to a modification of the central fringe amplitudes and a line pulling that complicates the determination of the exact line center. This difficulty becomes particularly severe in the case of high-resolution spectroscopy with laser-cooled atoms where this limits the accuracy obtainable [12]. In comparison, the calculated signals for the PSAB interferometer [see also Fig. 1(b)] show a pure singlet structure due to interference in the low-frequency
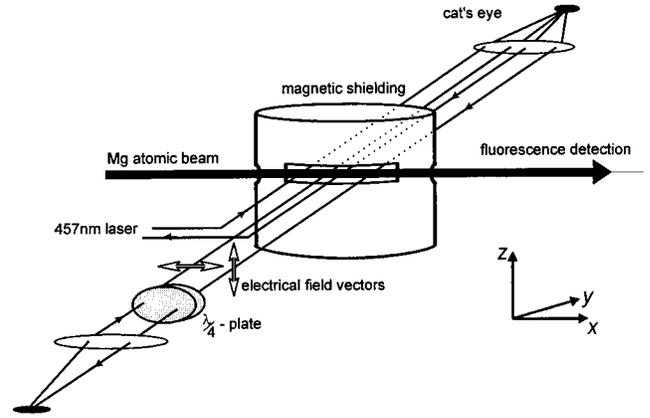


FIG. 3. Scheme of the experimental setup for the optical Ramsey interferometer with path-selective beam splitters.

component (solid squares in Fig. 2). In agreement with Eq. (5), both the incoherent background and the interference amplitude are increased. Due to the chromatic aberration, the contrast of the signals dropped considerably compared to the values calculated above for idealized beam splitters. A detailed discussion of the interference contrast will be given in the following section.

## IV. EXPERIMENTAL RESULTS AND DISCUSSION

Our interferometer setup consists of a thermal magnesium atomic beam with a mean velocity of about 700 m/s, which is crossed by two antiparallel pairs of traveling light waves (see also Fig. 3). The laser beams are resonant with the $^1S_0$-$^3P_1$ intercombination transition of $^{24}$Mg ($\lambda = 457$ nm, lifetime of the $^3P_1$ state $\tau = 5.1$ ms) and are generated by a high-resolution dye laser spectrometer. The parallelism of the laser beams is provided by two so-called cat's eyes. The inner two beams are passed through a $\lambda/4$ plate, which prepares a $\pi_x$ polarization for the electric-field vector of the laser. The number of excited atoms in the interferometer exits is measured by monitoring the fluorescence 0.3 m below the interaction region. The distance $D$ between the first and second and between the third and fourth laser beams is about $4.3 \times 10^{-3}$ m. Note that the distance between the second and third laser zones is not relevant because interfering arms propagate in the same state in this region. A magnetic shielding of the whole interferometry region protects from magnetic stray fields. Further experimental details are given in Refs. [7, 19].

Figure 4 shows typical experimental interference data for the two different configurations in Figs. 1(a) and 1(b). The measurement time per data point is 0.25 s in both cases. The filled squares represent signals from the PSAB interferometer. The open squares describe the two-level doublet signals. To compare the two schemes we numerically extracted that part of the signal coming from the low-frequency recoil component (solid line in Fig. 4). The central fringe contrast of the obtained singlet structure, determined from the amplitude of the main fringe divided by the background signal, is $(6.8 \pm 0.4)\%$. The shape of the experimental data is in excellent agreement with theory. Obviously, the high-frequency recoil component of the PSAB signal has completely disappeared and the signal is free from line-pulling effects. The
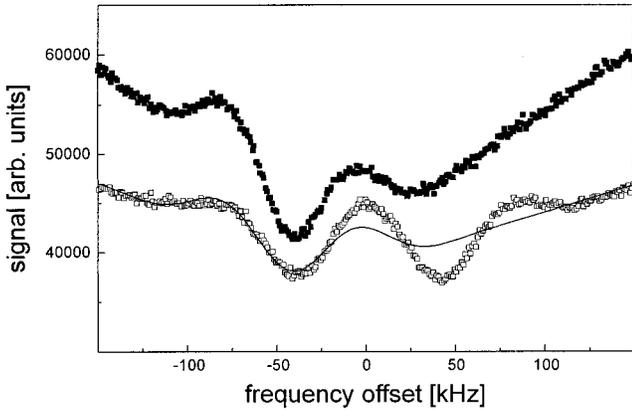
FIG. 4. Measured interference signals for the Ramsey-Bordé interferometer (open squares) and for the PSAB interferometer (solid squares). The solid line is that part of a fit which corresponds to the low-frequency component for the Ramsey-Bordé signal.

amplitude and background of the remaining low-frequency recoil component are increased. From the plotted data we compute a contrast of $(11.2 \pm 0.5)\%$ for the PSAB signal. The contrast of both signals is about 20% lower than predicted by the numerical calculations, which we suppose to be due to a slight misalignment of the laser beams. However, we observe a relative contrast gain of about 65% for the PSAB interferometer. As a further advantage the total level of the PSAB signal is higher by a factor of about 1.2. For our shot-noise limited signals this directly enters the signal-to-noise ratio due to the lower relative shot noise of the atomic number statistics.

The Ramsey-Bordé interferometer offers excellent opportunities for frequency standard applications [12,15,21,22]. For this kind of high-resolution spectroscopy exact knowledge about the influence of uncontrolled magnetic stray fields on the signals is of great importance. Therefore, in the following we will briefly discuss this subject.

The Zeeman shift of the $^3P_1$ state is $2.1 \times 10^4$ MHz/T. A special property of the PSAB configuration is that due to the symmetric excitation of the $m_z = +1$ and $-1$ levels all Zeeman shifts are symmetrical to the line center. Therefore, to first order no line shift appears in the signals. Neglecting the quadratic Zeeman effect of the $m_z = 0$ levels, the influence of magnetic fields is restricted to the small central region ($d = 2 \times 10^{-3}$ m) between the second and third laser beams where the $m_z = \pm 1$ levels are excited. Two different effects have to be considered.

The first effect is population transfer from the bright state $|e_c\rangle$ to the dark state $|e_{nc}\rangle$ due to a constant magnetic offset field. Because the dark state does not take part in the interference process this can be interpreted as a loss mechanism that reduces the interference contrast. We measured the offset magnetic fields within our magnetic shielding to be less than $10^{-7}$ T [19], leading to a relative dark state population of the order of $10^{-5}$. This loss mechanism can be neglected up to this order.

The second effect is orientation in the Zeeman sublevels of the $^3P_1$ state caused by imperfectly linear polarization of the four laser beams. For small fractions of $\sigma^+$- or $\sigma^-$-polarized light in the laser beams the populations of the $m_z = +1$ and $-1$ levels are different, which gives rise to a

line shift in the interference signal depending on the strength of magnetic offset fields. For an offset field less than $10^{-7}$ T the line shift for the excitation of only a single Zeeman sublevel is in the kilohertz regime. We use conventional polarizing optics for the preparation of our laser beams. The residual fraction of circularly polarized light in the beams should be smaller than $10^{-4}$, which is already sufficient to get an uncertainty of the line center in the sub-hertz regime due to this effect.

In conclusion, in our experiment magnetic stray fields neither reduce the interference contrast nor limit the accuracy of the line center.

## V. CONCLUSION

We have demonstrated an optical Ramsey interferometer working with multilevel path selective beam splitters. Although the method presented is based on well-known optical pumping processes, in the context of coherent atom optics it represents a key element for different atom interferometer geometries that have not been realized so far. In comparison to the original Ramsey-Bordé interferometer, our interference signals show pure singlet structures and are free of line-pulling effects due to the overlap within the typical doublet fringe systems. Other experiments on the suppression of one of the recoil components have already been done [7,20,23,24]. While these methods rely on the destruction of certain interferometer parts and are typically connected with a loss of contrast, we obtain a contrast improvement of about 65% for a single recoil component directly compared to the original Ramsey-Bordé interferometer. The extension of the presented concept to a pure Mach-Zehnder geometry using laser-cooled atoms with a narrow velocity distribution promises a further improvement of the signals up to a contrast of, in principle, 100%.

On the other hand, the concept presented in this paper can be extended beyond the scheme of Fig. 1(c). We will give two examples.

(a) The application of an additional series (with even numbers) of copropagating $\pi$ pulses with $\pi_z$ polarization after the first interaction zone and the same series with opposite direction before the last interaction zone (polarization sequence $\pi_z$-$\pi_z$-$\cdots$-$\pi_x$-$\pi_x$-$\cdots$-$\pi_z$-$\pi_z$ and optical pulse sequence $\pi/2$-$\pi$-$\cdots$-$\pi$-$\pi$-$\cdots$-$\pi$-$\pi/2$) represents a possibility to significantly enlarge the enclosed area of the interferometer. In that scheme, however, during the interaction with the additional pulses, both partial waves accumulate opposite ''photon momentum kicks.'' As a consequence, the distance between the two interfering paths is expanded. Due to the Doppler shifts developing divergently the number of additional excitations is limited by the spectral width of the excitation process. This scheme in principle also holds for a conventional two-level based Ramsey interferometer.

(b) A different, more sophisticated way to enlarge the interferometer area that takes advantage of the very concept of polarizing beam splitters is to apply an even number of more than two alternately propagating $\pi$ pulses with $\pi_x$ polarization (polarization sequence $\pi_z$-$\pi_x$-$\pi_x$-$\cdots$-$\pi_x$-$\pi_x$-$\pi_z$ and optical pulse sequence $\pi/2$-$\pi$-$\pi$-$\cdots$-$\pi$-$\pi$-$\pi/2$). The path-selective interaction allows for the compensation of the arising Doppler shifts by adjusting the frequency of the cor-

responding laser pulse. Thus the number of additional pulses and therefore the attainable enclosed area is in principle not limited. This appears to be of interest for the realization of improved atom-based Sagnac interferometers [25].

[1] *Atom Interferometry*, edited by P. Berman (Academic, New York, 1997).

[2] *High-Resolution Laser Spectroscopy*, edited by R. Blatt and W. Neuhauser (Springer, Berlin, 1994).

[3] O. Carnal and J. Mlynek, Phys. Rev. Lett. **66**, 2689 (1991).

[4] D. W. Keith, C. R. Ekstrom, Q. A. Turchette, and D. E. Pritchard, Phys. Rev. Lett. **66**, 2693 (1991).

[5] M. Kasevich and S. Chu, Phys. Rev. Lett. **67**, 181 (1991).

[6] F. Riehle, Th. Kisters, A. Witte, J. Helmcke, and C. J. Bordé, Phys. Rev. Lett. **67**, 177 (1991).

[7] U. Sterr, K. Sengstock, J. H. Müller, D. Bettermann, and W. Ertmer, Appl. Phys. B: Photophys. Laser Chem. **54**, 341 (1992).

[8] F. Shimizu, K. Shimizu, and H. Takuma, Phys. Rev. A **46**, R17 (1992).

[9] E. M. Rasel, M. K. Oberthaler, H. Batelaan, J. Schmiedmayer, and A. Zeilinger, Phys. Rev. Lett. **75**, 2633 (1995).

[10] D. M. Giltner, R. W. Mc Gowan, and S. A. Lee, Phys. Rev. Lett. **75**, 2638 (1995).

[11] S. B. Cahn, A. Kurmarakrishnan, U. Shim, T. Sleator, P. R. Berman, and B. Dubetsky, Phys. Rev. Lett. **79**, 784 (1997).

[12] K. Sengstock, U. Sterr, J. H. Müller, V. Rieger, D. Bettermann, and W. Ertmer, Appl. Phys. B: Lasers Opt. **59**, 99 (1994).

[13] K. Zeiske, G. Zinner, F. Riehle, and L. Helmcke, Appl. Phys. B: Lasers Opt. **60**, 205 (1995).

[14] A. Morinaga, T. Tako, and N. Ito, Phys. Rev. A **48**, 1364 (1993).

[15] Th. Kisters, K. Zeiske, F. Riehle, and J. Helmcke, Appl. Phys. B: Lasers Opt. **59**, 89 (1994).

[16] V. Rieger, K. Sengstock, U. Sterr, J. H. Müller, and W. Ertmer, Opt. Commun. **99**, 172 (1993).

[17] C. J. Bordé, Phys. Lett. A **140**, 10 (1989).

[18] C. J. Bordé, C. Salomon, S. Avrillier, A. van Lerberghe, C. Bréant, D. Bassi, and G. Scoles, Phys. Rev. A **30**, 1836 (1984).

[19] H. Hinderthür, A. Pautz, V. Rieger, F. Ruschewitz, J. L. Peng, K. Sengstock, and W. Ertmer, Phys. Rev. A **56**, 2085 (1997).

[20] F. E. Dingler, V. Rieger, K. Sengstock, U. Sterr, and W. Ertmer, Opt. Commun. **110**, 99 (1994).

[21] K. Sengstock, U. Sterr, G. Hennig, D. Bettermann, J. H. Müller, and W. Ertmer, Opt. Commun. **103**, 73 (1993).

[22] H. Schnatz, B. Lipphardt, J. Helmcke, F. Riehle, and G. Zinner, Phys. Rev. Lett. **76**, 18 (1996).

[23] F. Riehle, J. Ishikawa, and J. Helmcke, Phys. Rev. Lett. **61**, 2092 (1988).

[24] T. Kurosu and A. Morinaga, Phys. Rev. A **45**, 4799 (1992).

[25] T. L. Gustavson, P. Bouyer, and M. A. Kasevich, Phys. Rev. Lett. **78**, 2046 (1997).